CRYSTAL GROWTH & DESIGN
2008
VOL. 8, NO. 6
1916–1923

# Capping Modes in PVP-Directed Silver Nanocrystal Growth: Multi-Twinned Nanorods versus Single-Crystalline Nano-Hexapods

Xiaohua Liu, Fan Zhang, Rui Huang, Caofeng Pan, and Jing Zhu*

*Beijing National Center for Electron Microscopy and Laboratory of Advanced Materials, Department of Materials Science and Engineering, Tsinghua University, Beijing 100084, China*

*Received November 15, 2007; Revised Manuscript Received January 20, 2008*

**ABSTRACT:** Silver nanostructures with different morphology and crystal structure are successfully synthesized using poly(vinyl pyrrolidone) (PVP) molecules with different molecular weight (MW) in the polyol process. Multitwinned nanorods and single-crystalline nanohexapods are obtained using PVP-H (MW ≈ 1 300 000) and PVP-L (MW ≈ 30 000), respectively. The nanorods and the nanohexapods both have face-centered cubic (FCC) crystal structures but with different lattice constants, i.e., $a = 4.0862$ Å for the nanorods and $a = 9.6193$ Å for the nanohexapods. The growth mechanism for the Ag nanostructures is studied in details. The control on the shape and the crystal structure is attributed to the different capping modes for the PVP-directed Ag nanocrystal growth.

## Introduction

Nonspherical silver (Ag) nanostructures have attracted considerable attention because of their shape-dependent properties and potential applications in a widespread of fields including plasmonics,[1] nanoelectronics[2] and bio/chemical sensing.[3–7] So far, many Ag nanostructures have been successfully synthesized with various morphologies such as spheres,[8] prisms,[9] rods/wires,[10–13] cubes,[14–16] belts,[17] hyperbranched disks,[18] and octahedra.[5] Most of the Ag nanostructures have a face-centered cubic (FCC) crystal structure as bulk FCC-Ag with a few exceptions.[11,17,19,20] Many of these nonspherical Ag nanostructures were produced using wet chemical methods.[1–10,12–15,17,21] Capping molecules are usually employed in these syntheses to direct an anisotropic crystal growth.[22] Although many well-defined nanocrystals have been synthesized, the essential mechanism of the organic−inorganic interaction involved remains ambiguous. A good example is the polyol synthesis of the Ag nanostructures using poly(vinyl pyrrolidone) (PVP) as the capping molecules.[5,10,13,14,22,23] It has been proposed that the PVP molecules selectively interact with the FCC-Ag {100} facets, resulting in twinned FCC-Ag nanorods in high yield.[22] The as-prepared nanorods show a unique 5-fold symmetry, but their crystal structure remains unchanged, i.e., FCC-Ag as the bulk. However, we recently reported a novel AgNH (AgNH = Ag nanohexapod) nanoparticle synthesized using a similar polyol process.[23] The structure and the optical properties of the AgNHs were studied. The AgNHs have a unique concave shape and a novel FCC crystal structure significantly differing from the FCC-Ag nanostructures previously reported.[23] Since the Ag nanostructures are very different from each other, it is worthy to study the growth process of the PVP-directed Ag nanocrystal syntheses. By comparing the different nanostructures obtained, we may find out the factors affecting the final products.

In this paper, we report the Ag nanocrystal growth directed by the PVP molecules with different molecular weight (MW). The FCC-Ag nanorods and the novel AgNHs were obtained using the PVP-H (MW ≈ 1 300 000) and the PVP-L (MW ≈ 30 000) molecules, respectively. We studied the shape evolution of the AgNHs in comparison with the multitwinned FCC-Ag nanorods. Finally, we proposed different capping

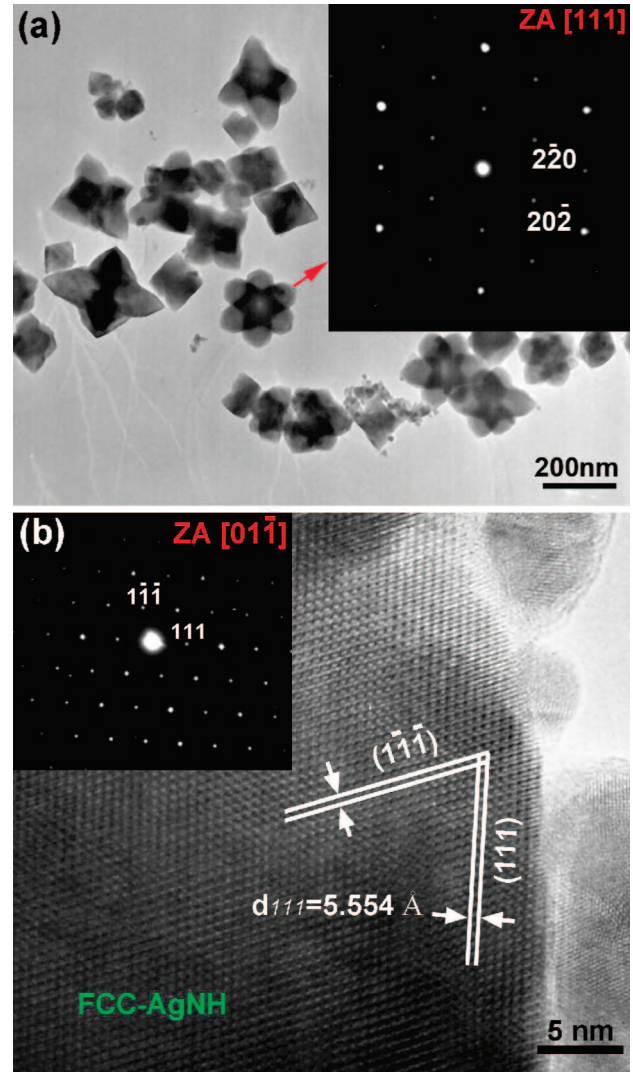


**Figure 1.** AgNHs produced using PVP-L. (a) A typical TEM image. The inset SAED pattern with a zone axis (ZA) of [111] is from the single-crystalline AgNH marked by the red arrow. (b) HREM image of the AgNH with a ZA of [00$\bar{1}$] proved by the inset SAED pattern. The spacing of the {111} planes is 5.554 Å.

* Corresponding author. E-mail: jzhu@mail.tsinghua.edu.cn.

10.1021/cg701128b CCC: $40.75 
Published on Web 05/03/2008

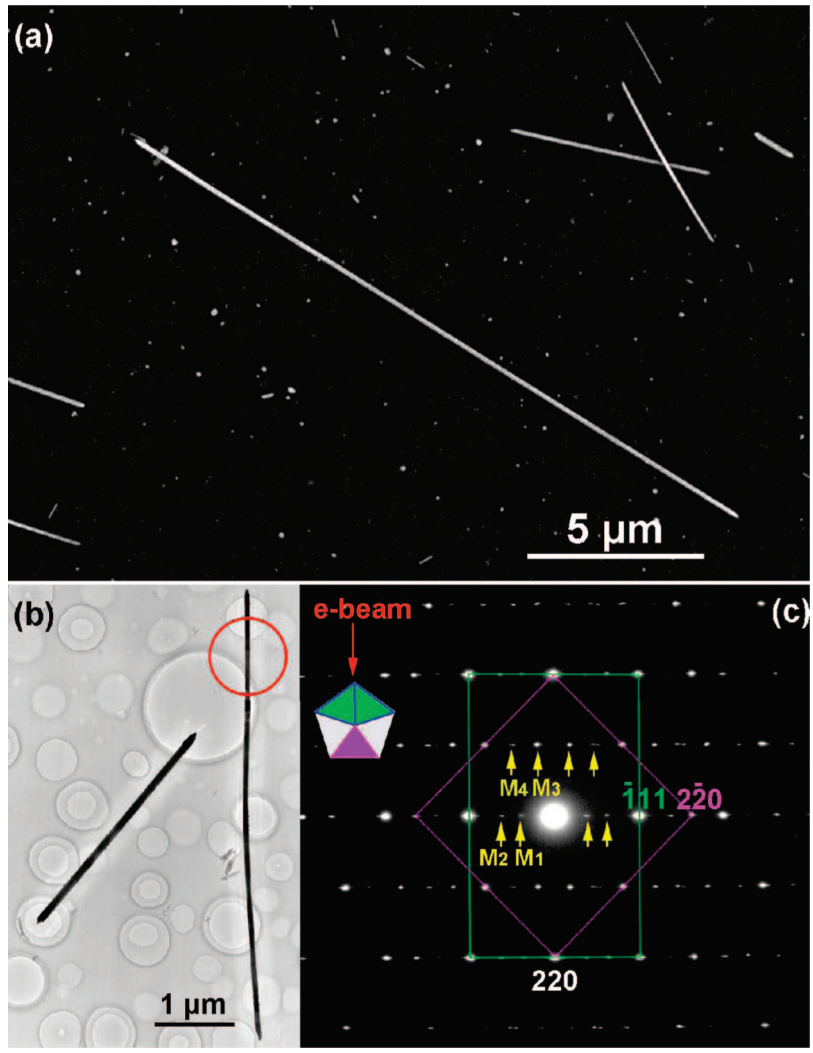


**Figure 2.** Multitwinned FCC-Ag nanorods produced using PVP-H. (a) A typical SEM image of the straight nanorods. (b) TEM image of two nanorods with sharp tips. (c) The SAED pattern from the nanorod marked by the red circle in (b). This pattern reveals the 5-fold cyclic twinning nature of the FCC-Ag nanorod shown by the inset scheme. The green rectangle indicates diffraction spots from two green subunits with a zone axis (ZA) of $[1\bar{1}2]$ and the purple square from the purple subunit with ZA [001]. The weak spots (M1−M4, marked by the yellow arrows) appear to be due to the double-diffraction effect of the superimposed subunits.

modes of the PVP molecules to interpret the remarkable differences of the Ag nanostructures produced using the similar polyol process.

## Experimental Section

**Reagents.** The following reagents were used as purchased without further purification: $AgNO_3$ (analytical reagent), PVP (MW ≈ 1 300 000 or MW ≈ 30 000, nominated respectively as PVP-H or PVP-L) and ethylene glycol (EG, analytical reagent).

**Synthesis of FCC-Ag Nanorods.** We used a modified synthetic route first developed by Sun and Xia to produce FCC-Ag nanorods.[13,15] $AgNO_3$ was reduced by EG in the presence of PVP-H molecules serving as the capping agents. No seeds were used in our synthesis. For a typical synthesis, 0.48 g of $AgNO_3$ and 0.48 g of PVP-H were dissolved separately in 15 mL of EG. The two solutions were both immediately subjected to vigorous stirring at room temperature (~25 °C) with magnetic blenders. A three-necked round-bottom flask containing 15 mL of EG was heated also with vigorous stirring. The temperature was maintained at ~158 °C by employing a thermo-controller. Then the $AgNO_3$/EG and PVP/EG solutions were injected dropwise and slowly into the hot EG simultaneously over a period of ~15 min. During slow injection of the reagents, the temperature of reaction system did not change obviously. Then the mixture was kept at ~158 °C for 10 h. Vigorous stirring was maintained through the entire process. The final product was a gray suspension containing twinned Ag nanorods.

**Synthesis of FCC-AgNHs and Their Derivatives.** The procedure used for production of the nanoparticles was slightly modified compared to as for the nanorods.[23] PVP-L of lower polymerization was used and the injection rate was much higher. The injection of $AgNO_3$/EG and PVP-L/EG solutions into the hot EG solvent was finished in 3 min. The use of PVP-L and the fast injection rate were found to be critical to produce the well-defined nanoparticles with the novel FCC-AgNH structure. We also obtained FCC-Ag nanorods using PVP-L with very slow injection rates. However, we failed to obtain well-defined nanoparticles using PVP-H even at low injection rates. So both low-polymerization PVP and high injection rate are necessary and the former is more important for the production of the AgNHs. AgNHs with obvious branches were produced as major products in very high yield, whereas some convex particles such as octahedra without branches were also observed, giving some information on the growth mechanism and shape evolution of the nanoparticles.

In order to study the shape evolution and growth mechanism of faceted nanoparticles, the as-synthesized AgNHs were placed in the PVP-L/$AgNO_3$/EG solution again. The mixture was kept at room

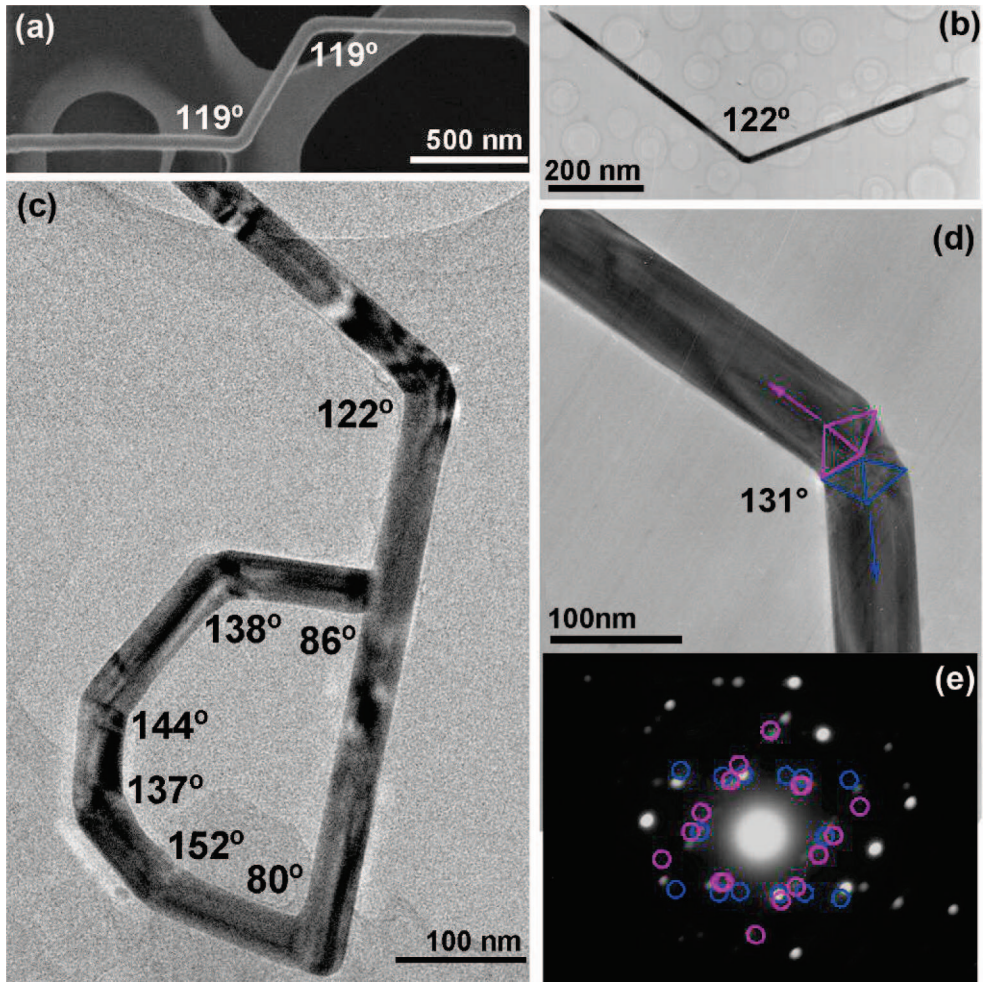


**Figure 3.** Zigzag FCC-Ag nanorods. (a) A Z-shaped nanorod. Two end arms are parallel to each other, both having an angle of 119° with the medium section. (b) A V-shape nanorod with a 122° angle between its two arms. (c) A d-shaped nanorod with many turnings of various turning angles. The diameter of the nanorod is uniform (~40 nm) and a nanoring is formed with a diameter of ~200 nm. (d) The junction of a zigzag nanorod and (e) its SAED pattern. It can be regarded as two twinned nanorods connected with an angle of 131°.

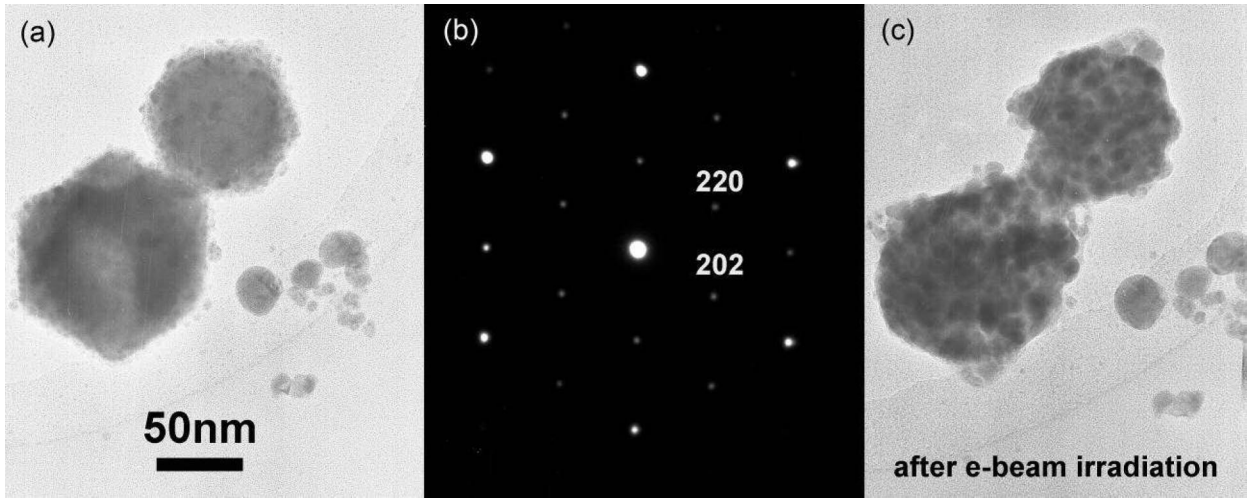


**Figure 4.** Single-crystalline seeds of the AgNHs. (a) Two seeds without any branches before electron beam irradiation. (b) The SAED pattern from the seed in (a). It shows that the seeds are single crystals with the identical crystal structure as the AgNHs. (c) After long irradiation time, the two seeds decay to FCC-Ag nanocrystals, showing the same metastability as the AgNHs.

temperature for 1 week. We observed an obvious increment in dimension of the AgNHs, resulting in a multipod-like branched morphology.

**X-ray Photoelectron Spectroscopy (XPS) of the AgNHs.** In order to investigate interaction of the PVP-L molecules and the Ag atoms in the AgNHs, XPS experiments were carried out by using the spectrometer PHI Quantera SXM (ULVAC-PHI, Inc.) with an Al $K_\alpha$ irradiation source (X photon energy of 1486.6 eV).

**Morphology and Crystal Structure Characterizations.** Electron micrographs were taken with scanning electron microscopes (SEM,

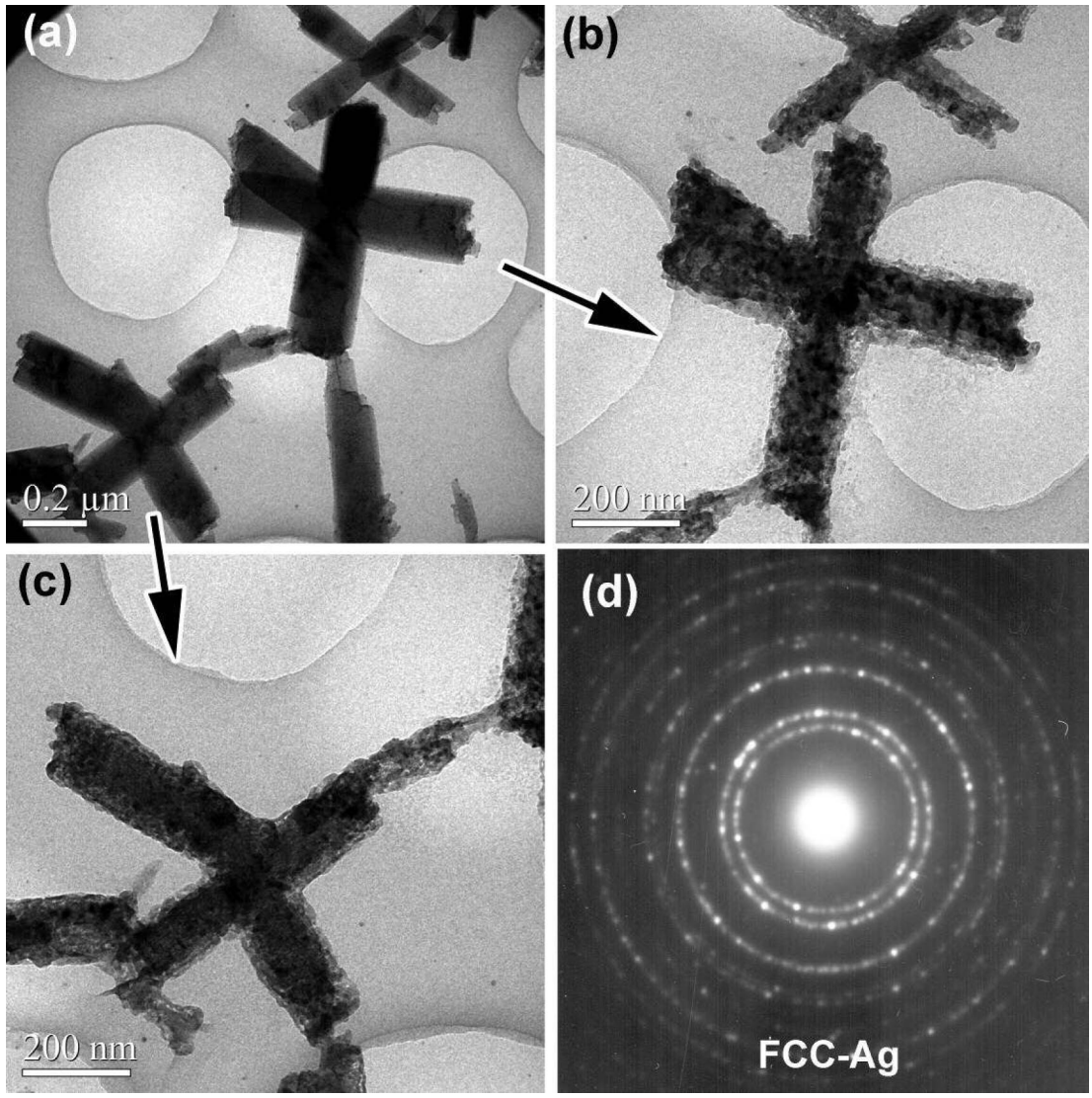


**Figure 5.** Decay of the multipods under electron beam irradiation. (a) The multipods are grown from the AgNHs with longer reaction time at room temperature by protruding their branches. The size is larger than that of the AgNHs and the seeds. The surfaces are smooth before irradiation. (b, c) After irradiation, the surfaces of the multipods become rough and the multipods decay to FCC-Ag crystallites, proved by (d) the SAED pattern indexed to FCC-Ag. This metastability is also similar to the seeds and the AgNHs.

JEOL JEM-6301F, or HITACHI S-5500) and transmission electron microscopes (TEM, JEOL JEM-2010F). Crystal structure of the products was studied using X-ray diffraction (XRD, using Riguku D/max-RB with a Cu $K_\alpha$ irradiation source), selected-area electron diffraction (SAED), and high-resolution electron microscopy (HREM).

## Results and Discussion

**Morphology and Crystal Structure.** Figure 1a shows the typical TEM image of the novel FCC-AgNH particles synthesized using the PVP-L as capping agents. The red arrow marks an AgNH particle with six branches. The SAED pattern from this AgNH is shown inset, with a zone axis (ZA) of [111]. Generally, the AgNHs exhibit various profiles due to different orientations with respect to the electron beam. The crystal structure of the AgNHs have been studied in details by us.[23] They possess a novel FCC-AgNH crystal structure ($a = 9.6193$ Å), very different from that of the FCC-Ag ($a = 4.0862$ Å).[23] Figure 1b shows the HREM image of an AgNH with ZA [00$\bar{1}$]. The large spacing of FCC-AgNH {111} planes can never be observed in FCC-Ag, further proving the AgNHs being new products by the polyol process. The yield of the AgNHs can be as high as 95%. Some smaller octahedral nanoparticles without branches are the byproducts (with percentage of ~5%), regarded as precursors of the AgNHs.

Figure 2 shows crystallographic characteristics of the FCC-Ag nanorod synthesized using PVP-H molecules as capping agents. The nanorods are very straight and have high aspect ratio (Figure 2a). The ends of the rods are usually tapering tips (Figure 2b). Electron microscopy analysis shows that the straight nanorod has the FCC-Ag crystal structure as the bulk, but with a distinguished crystallographic feature of 5-fold twinning. Five cyclically twinned subunits (all FCC-Ag crystals) share a common $\xi$ axis (also the axis of the nanorod). This structure is confirmed by the SAED pattern (Figure 2c). Because of superposition of the subunits, the additional diffraction spots (M1−M4) are also observed and attributed to second diffraction effects.[24–29] The unique 5-fold twinning of the FCC-Ag nanorods has been suggested to arise from selective interaction between the PVP-H molecules and {100} planes. An anisotropic growth of the nanorod is achieved by deposition of Ag atoms onto the pyramidal tip terminated by {111} planes.[13,22,30]

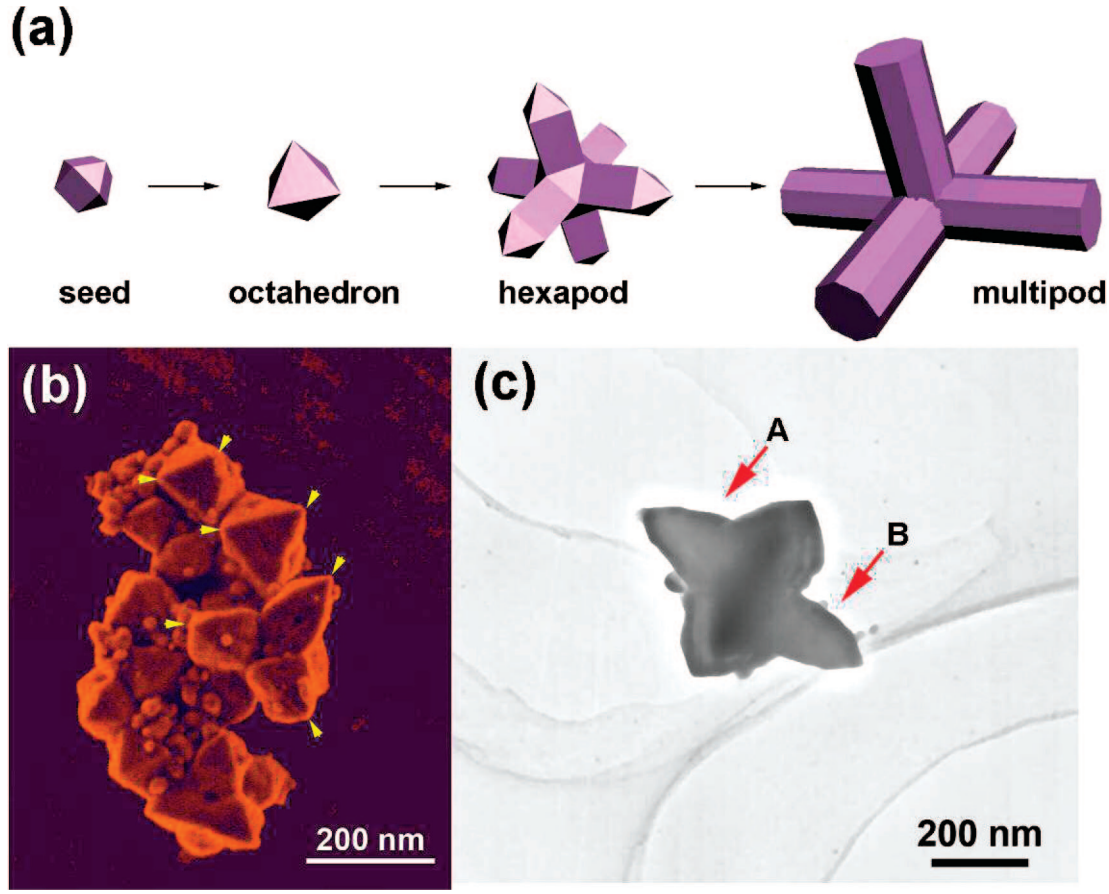


**Figure 6.** Shape evolution of the AgNHs. (a) Schematic illustration for an ideal growth process. An equilibrium cuboctahedral seed develop to an octahedron, then a hexapod, and finally to a multipod-like particle. (b) Different morphologies in the AgNHs aggregates. Three particles marked by the yellow triangles have different sizes. The small seed has smallest size and a convex shape, whereas the hexapod has the largest size and obvious branches. (c) An asymmetric AgNH particle. Note the different thickness of the opposite branches marked by red arrows A and B, which indicates lateral growth of the branches accompanying protrusion of the tips. The branch marked by Arrow B should represent the ideal shape of a hexapod without lateral growth illustrated in (a).

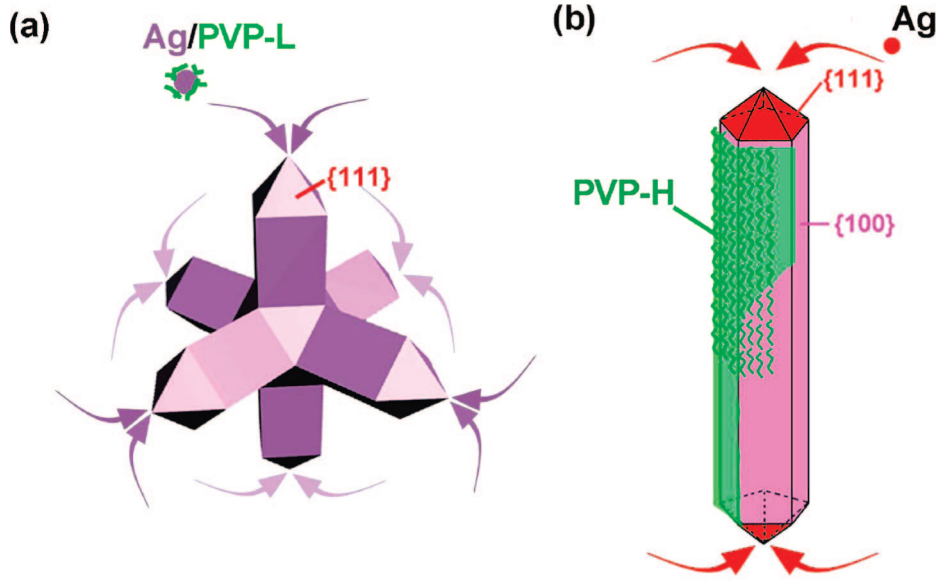


**Figure 7.** Schematic illustration of the different capping modes for the PVP-directed Ag nanocrystal growth. (a) Inner capping mode for the AgNHs. Ag clusters and the PVP-L molecules co-deposit onto the six pyramidal tips of the AgNH. Thus PVP-L molecules are packed into the AgNH lattice. (b) Outer capping mode for the 5-fold twinned FCC-Ag nanorods. The PVP-H molecules interact with the lateral {100} surfaces. Only Ag clusters deposit onto the pentagonal pyramids at two ends of the nanorod. There is no room for the organic molecules inside the close-packed lattice of the FCC-Ag nanorods.

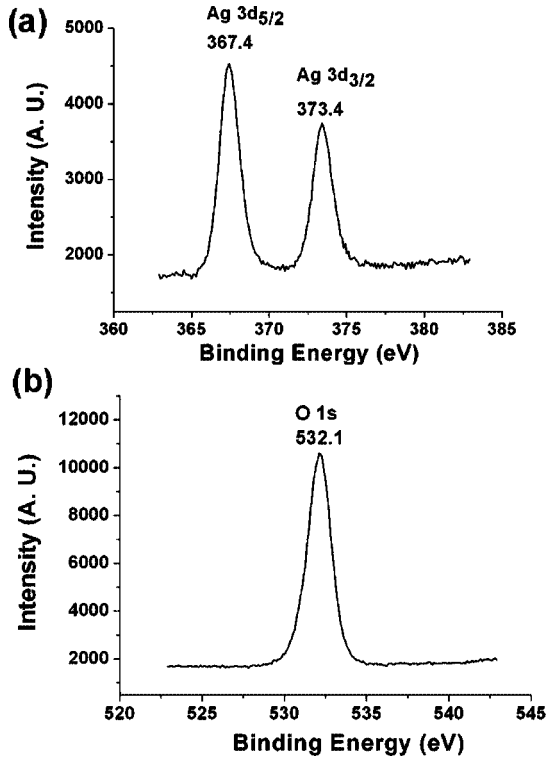


**Figure 8.** XPS spectra of AgNHs. (a) XPS for Ag 3d electrons. The two peaks both shift 0.9 eV down to lower binding energy compared to $Ag^0$. (2) XPS for O 1s electrons. The peak shifts 1.8 eV up to higher binding energy compared to that for pure PVP.

Novel zigzag FCC-Ag nanorods are also found as a minor product in the sample produced using PVP-H as capping agents. Figure 3 shows the typical images of these nanorods, i.e. a Z-shaped rod (Figure 3a), a V-shaped rod (Figure 3b) and a d-shaped rod (Figure 3c). All these nanorods have the same FCC-Ag crystal structure as the straight nanorods, as proved by electron diffraction studies (panels d and e in Figure 3). A zigzag FCC-Ag nanorod has uniform diameter all long but with at least one turning. The turning angles spread in a large range (mainly obtuse angles, ~90−180°). Occasionally many turnings can be seen in a thin nanorod (Figure 3c). Many short segments with uniform thickness are connected, forming a nanoring with a diameter of ~200 nm at the end. Although nanorings have been found in some oxide nanomaterials such as ZnO,[31] this very interesting nanoring has seldom been observed in metals. Gao and his co-workers reported the turning angles in a large range of 90−170°. They also speculated a self-assembly growth mechanism of the Z-shaped rods based on the formation of straight nanorods.[25] However, we find that the turning angles are much more abundant in the range of 110−150° than those with either smaller or larger angles (see the Supporting Information, Figure S1). Electron microscopic analysis reveals that a Z-shaped nanorod can be grown by elongation of two opposite tetragonal tips of a decahedral 5-fold-twinned seed (panels d and e in Figure 3). This is another reasonable mechanism for the formation of the zigzag nanorods. However, this may not account for all turning angles especially for the d-shaped nanorod. Further crystallographic studies are necessary to get a comprehensive understanding of the formation mechanism.

The products of the polyol process using the PVP-H molecules can be FCC-Ag nanoparticles, straight nanorods or zigzag nanorods, depending on reaction parameters. Typical yields for the FCC-Ag nanostructures can be ~15% nanoparticles, ~70% straight nanorods and ~15% zigzag nanorods.

**Growth Mechanism of the AgNHs.** The growth mechanism of FCC-Ag nanostructures has been widely studied.[30] However, the growth mechanism of the unique AgNHs has not been studied yet.[23] This problem should be well-addressed before we study the controlled syntheses of the Ag nanostructures using different PVP molecules.

Because of the very high yield and the fast formation of the AgNHs, we can observe only some small nanoparticles as byproducts in the sample with yield of ~5%. The typical size of these convex nanoparticles is ~100 nm, smaller than the branched AgNHs. They have octahedral or truncated octahedral shapes based on SEM observations. These nanoparticles are also single-crystalline and have the same crystal structure before intense electron-beam irradiation (panels a and b in Figure 4). They are also metastable as the AgNHs, decaying to FCC-Ag crystallites after irradiation (Figure 4c). Thus the AgNHs are most probably grown from these "seeds".

To complete the growth process, we again placed the as-prepared AgNHs into the reagent mixture (PVP-L/$AgNO_3$/EG) for a week. As a result, unique multipods were obtained (Figure 5a). They also have smooth surfaces and well-defined geometry but much larger dimensions than the AgNHs. They are also metastable under electron beam irradiation and decay to FCC-Ag nanoparticles (Figures 5b−d). The yield of the multipods is almost 100% because of the pure AgNHs seeds and very long reaction time.

We can clearly see a complete process of nanocrystal growth formed by the small convex seeds, the faceted AgNHs, and the multipods. The shape evolution of the nanocrystals with the FCC-AgNH structure is illustrated in Figure 6a. The equilibrium shape for a free FCC crystal is a cuboctahedron (seed).[32] Because the {111} planes in FCC crystals have the lowest surface energy, an octahedron is also a possible shape for the AgNH crystals with small sizes. By elongation of the six pyramidal tips of an octahedron, it evolves to a branched hexapod. With the deposition of the Ag clusters and the capping molecules, a hexapod develops to a multipod-shaped particle with thick branches. The multipods are usually less faceted than the AgNHs. Some branches may be broken and lost during the sample preparations. However, the geometrical relation remains in the remnant parts, i.e., adjacent branches forming a right angle. Figure 6b shows a high-resolution SEM image of the nanoparticles at different stages of the growth. The yellow triangles indicate the tips as growing sites. A branched nanostructure is form by elongation of the tips at six equivalent <100> directions. There is also lateral growth of the branches, resulting in a thicker base and a thinner tip of the branches. This lateral growth is confirmed by a very unusual asymmetric AgNH (Figure 6c). The "B" branch has a column shape, in contrast to the "A" branch with a tapering shape. The lateral growth rate must be much lower than the tip elongation rate according to the geometry of the AgNHs. Note that the lateral growth is not illustrated in the scheme (Figure 6a).

**Capping Mode.** On the basis of the above investigations, we can see that the PVP-L molecules direct an isotropic packing along six branches of the FCC-AgNHs. Structure analyses have indicated that the FCC-AgNHs have a bicontinuous structure and very low packing density.[23] In contrast, the PVP-H molecules direct a one-dimensional growth of the FCC-Ag nanorods. The FCC-Ag nanorods have a close-packed structure and thus no room for the PVP-H molecules packing into the

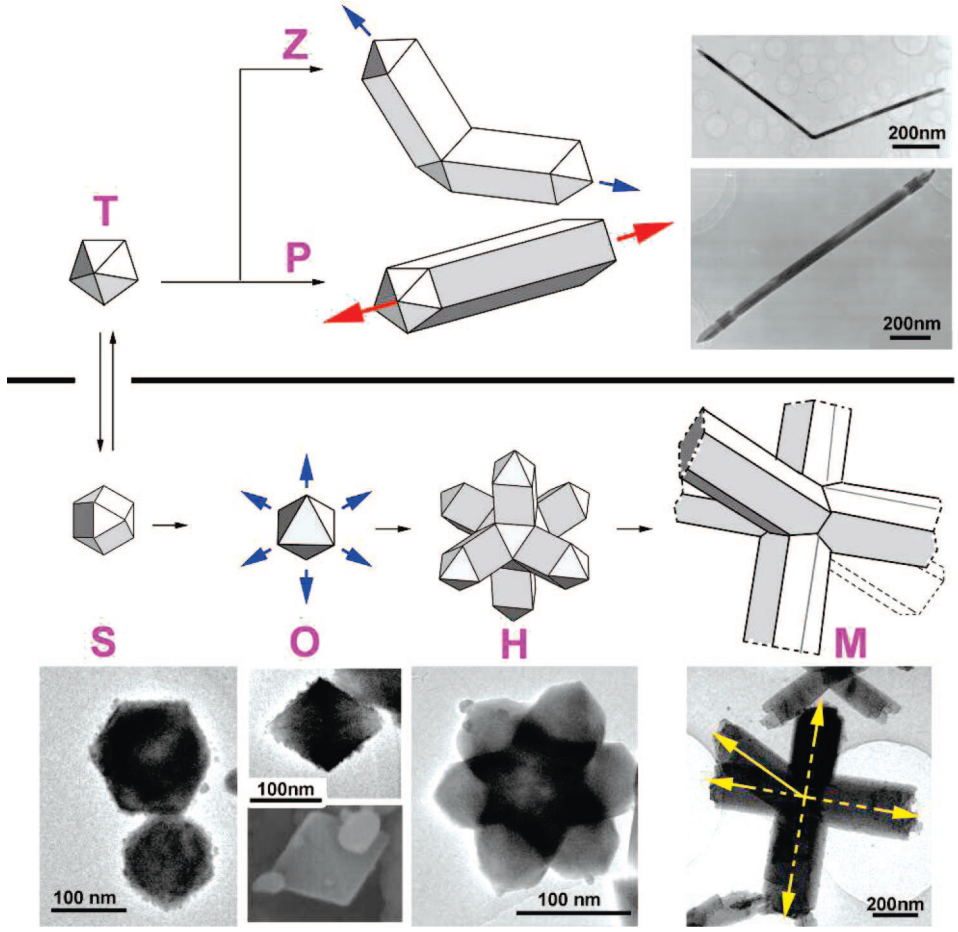


**Figure 9.** General growth mechanism of the Ag nanostructures. At the nucleation stage, a seed fluctuates between the twinned (marked as "T") and the single-crystalline ("S") structures with a decahedral and a cuboctahedral shape, respectively. The T-seeds can grow either to zigzag ("Z") or straight pentagonal ("P") nanowires by elongation at different pyramidal tips (marked by the blue and red arrows). An S-seed can evolve to form an octahedron ("O"), a hexapod ("H"), and a multipod ("M"). Experimentally these nanostructures with different morphologies are obtained and shown nearby. The yellow arrows show the branches of the multipods. In general, the growth takes place at the pyramidal tips bounded by several {111} planes.

lattice. So we speculate that different capping modes have operated in our syntheses.

For the AgNH serious including octahedral, hexapod-like and multipod-like nanoparticles, PVP-L molecules and the Ag clusters co-deposit onto six tips of the AgNH (Figure 7a). The PVP-L molecules interact with the $Ag_6$ octahedra in the bicontinuous lattice,[23] stabilizing the Ag skeleton of low packing density. The polymer molecules serve as linkers of inorganic clusters and are packed into the lattice. This results in an organic−inorganic hybrid nanocomposite, similar to a metal-organic framework (MOF).[33] We define this interaction between the PVP-L molecules and the Ag clusters as an "inner" capping mode, i.e., it operates at atomic scale inside the lattice.

For the FCC-Ag nanorods with high packing density, there is no room in the lattice for the PVP-H molecules. The PVP-H molecules interact with the outer {100} surfaces (Figure 7b).[29] Unlike the PVP-L molecules, the PVP-H molecules do not influence the atomic arrangement inside the lattice. Thus these nanorods preserve the FCC-Ag structure and are quite stable under intense electron-beam irradiation. The PVP-H molecules serve as a "soft template" to direct the anisotropic growth of the FCC-Ag nanorods. The assembly of PVP layers on the FCC-Ag nanorods has been suggested by several authors,[22,29,30] consistent with our investigations. Intriguingly, this "outer" capping mode is confirmed by formation of the $Ag_2S$ nanotubes by exposing the FCC-Ag nanorod in the open air for 2−3 weeks (see the Supporting Information, Figure S2).

We also study the X-ray photoelectron spectrum (XPS) of the AgNHs to further understand the interaction between the PVP-L molecule and the $Ag_6$ octahedra (Figure 8). Two peaks occur at 367.4 and 373.4 eV, corresponding to the binding energies of Ag $3d_{5/2}$ and Ag $3d_{3/2}$, respectively. In comparison with $Ag^0$ (368.3 and 374.3 eV),[8,29] the peaks shift down to lower binding energy (−0.9 eV), indicating the chemical environment of the Ag atoms is changed. Figure 8b shows the O 1s peak appearing at 532.1 eV, much higher (+1.8 eV) than 530.3 eV in pure PVP. This negative shift for Ag 3d peak and positive shift for O 1s indicate strong Ag:O coordination, consistent with the repeated $Ag_6$ octahedra in the AgNH lattice and functional group >C═O in the PVP chains.

It is interesting that only PVP-L molecules with lower polymerization operated for the inner capping mechanism. The reason is still ambiguous at present. We note that PVP-H has much longer chains than PVP-L, it seems more reasonable for a shorter chain inserted into the channel of the AgNHs than a longer chain. From a viewpoint of crystal growth, it may be related to possible different solution structure in the $AgNO_3$/PVP/EG reaction mixture. This would be an interesting topic for crystal engineering.

**General Growth Mechanism of the Ag Nanostructures.** Now we can draw the synthetic roadmap for both the twinned FCC-Ag nanorods and single-crystalline FCC-AgNH nanoparticles (Figure 9). At the nucleation stage, a seed fluctuates between the twinned (marked as "T") and the single-crystalline ("S") structures with a decahedral and a cuboctahedral shape,[34,35] respectively. The T-seeds can grow either to zigzag ("Z") or straight pentagonal ("P") nanorods by elongation at different pyramidal tips (marked by the blue and red arrows). An S-seed can evolve to form an octahedron ("O"), a hexapod ("H"), and a multipod ("M"). Experimentally these nanostructures with different morphologies are obtained and shown near the corresponding shapes. The yellow arrows show the branches of the multipods. In general, the growth takes place at the pyramidal tips bounded by several {111} planes. PVP-H show stronger ability to direct anisotropic growth than PVP-L.

This map for the growth of various Ag nanostructures could also be interpreted qualitatively with an energetic viewpoint. At the initial stage, the $Ag^+$ ions are reduced to Ag atoms that further agglomerate into small clusters. The seeds can be formed by atomic addition or random combination of these clusters. However, the shape of a seed is determined by the requirement of the minimum surface energy. Because all the interfaces and surfaces are {111} planes in the multitwinned particles (MTPs), they are known as alternative low-energy structures as the S-seeds.

The Ag nanostructures are grown from the T- or S-seeds by atomic addition. The Ag atoms and clusters selectively deposit onto a seed at the higher-energy sites, i.e., vertices and edges of a seed. Ag atoms preferentially deposit at the pentagonal pyramids with 5 edges meeting (marked by the red arrows in Figure 9). If the {100} planes have been capped by the PVP-H molecules, a P-nanorod can preserve the structure with all surfaces and interfaces being {111} planes. So the P-nanorods are energetically favorable than the Z-nanorod. This accounts for the higher yield of the P-nanorods than the Z-nanorods in the FCC-Ag nanostructures. For the O-nanoparticle, there are six equivalent pyramidal tips (marked by the blue arrows in Figure 9). Thus the growth takes place at all these sites, leading to formation of six branches. The PVP-L molecules do not cap on the outer surfaces of the AgNHs, thus the lateral growth is observed as shown in Figure 6c.

## Conclusions

In summary, we have synthesized the Ag nanostructures with different morphologies and crystal structures, including straight and zigzag nanorods, octahedral, hexapod- and multipod-like nanoparticles. The nanorods have the FCC-Ag crystal structure as bulk Ag ($a = 4.0862$ Å), while the nanoparticles have a novel FCC structure with a much larger lattice constant ($a = 9.6193$ Å). The growth mechanism of the AgNHs is studied. The difference in morphology is related to the capping modes of the PVP molecules with different molecular weights. The PVP-H (MW $\approx$ 1 300 000) molecules interact with the outer surfaces of the nanorods (an outer capping mode), resulting in an anisotropic growth of FCC-Ag multitwinned nanorods. The PVP-L (MW $\approx$ 30 000) molecules interact with Ag clusters inside the lattice, forming organic−inorganic nanocomposite with the large unit cell. Shape evolution from the octahedra through hexapods to multipods is achieved by codeposition of the PVP-L molecules and the Ag clusters.

**Acknowledgment.** This work was supported by the National 973 Project of China, National Natural Science Foundation of China, and National Center for Nano-Science and Technology of China.

**Supporting Information Available:** SEM and TEM images for zigzag nanorods (Figure S1); formation of a silver sulfide nanotube indicating the presence of PVP-H layers on the surfaces of the FCC-Ag nanorod (Figure S2); experimental and simulated XRD spectra of the AgNHs (Figure S3); SEM image of the AgNHs showing their high yield (Figure S4) (PDF). This material is available free of charge via the Internet at http://pubs.acs.org.

## References

(1) Tao, A.; Sinsermsuksakul, P.; Yang, P. *Nat. Nanotechnol.* **2007**, *2*, 435–440.
(2) Wiley, B. J.; Wang, Z. H.; Wei, J.; Yin, Y. D.; Cobden, D. H.; Xia, Y. N. *Nano Lett.* **2006**, *6*, 2273–2278.
(3) Wiley, B. J.; Chen, Y.; McLellan, J. M.; Xiong, Y.; Li, Z.-Y.; Ginger, D.; Xia, Y. *Nano Lett.* **2007**, *7*, 1032–1036.
(4) McLellan, J. M.; Li, Z. Y.; Siekkinen, A. R.; Xia, Y. N. *Nano Lett.* **2007**, *7*, 1013–1017.
(5) Tao, A.; Sinsermsuksakul, P.; Yang, P. D. *Angew. Chem., Int. Ed.* **2006**, *45*, 4597–4601.
(6) Tao, A.; Kim, F.; Hess, C.; Goldberger, J.; He, R. R.; Sun, Y. G.; Xia, Y. N.; Yang, P. D. *Nano Lett.* **2003**, *3*, 1229–1233.
(7) Xia, Y. N.; Halas, N. J. *MRS Bull.* **2005**, *30*, 338–344.
(8) Huang, H. H.; Ni, X. P.; Loy, G. L.; Chew, C. H.; Tan, K. L.; Loh, F. C.; Deng, J. F.; Xu, G. Q. *Langmuir* **1996**, *12*, 909–912.
(9) Jin, R. C.; Cao, Y. W.; Mirkin, C. A.; Kelly, K. L.; Schatz, G. C.; Zheng, J. G. *Science* **2001**, *294*, 1901–1903.
(10) Sun, Y. G.; Xia, Y. N. *Adv. Mater.* **2002**, *14*, 833–837.
(11) Liu, X. H.; Luo, J.; Zhu, J. *Nano Lett.* **2006**, *6*, 408–412.
(12) Sun, X. M.; Li, Y. D. *Adv. Mater.* **2005**, *17*, 2626-+
(13) Sun, Y. G.; Yin, Y. D.; Mayers, B. T.; Herricks, T.; Xia, Y. N. *Chem. Mater.* **2002**, *14*, 4736–4745.
(14) Siekkinen, A. R.; McLellan, J. M.; Chen, J. Y.; Xia, Y. N. *Chem. Phys. Lett.* **2006**, *432*, 491–496.
(15) Sun, Y. G.; Xia, Y. N. *Science* **2002**, *298*, 2176–2179.
(16) Sherry, L. J.; Chang, S. H.; Schatz, G. C.; Van Duyne, R. P.; Wiley, B. J.; Xia, Y. N. *Nano Lett.* **2005**, *5*, 2034–2038.
(17) Huang, T. K.; Cheng, T. H.; Yen, M. Y.; Hsiao, W. H.; Wang, L. S.; Chen, F. R.; Kai, J. J.; Lee, C. Y.; Chiu, H. T. *Langmuir* **2007**, *23*, 5722–5726.
(18) Lou, X. W.; Yuan, C. L.; Archer, L. A. *Chem. Mater.* **2006**, *18*, 3921–3923.
(19) Liang, C. H.; Terabe, K.; Hasegawa, T.; Aono, M. *Jpn. J. Appl. Phys., Part 1* **2006**, *45*, 6046–6048.
(20) Taneja, P.; Banerjee, R.; Ayyub, P.; Dey, G. K. *Phys. Rev. B* **2001**, *6403*, 033405.
(21) Wiley, B. J.; Xiong, Y. J.; Li, Z. Y.; Yin, Y. D.; Xia, Y. N. *Nano Lett.* **2006**, *6*, 765–768.
(22) Wiley, B.; Sun, Y. G.; Chen, J. Y.; Cang, H.; Li, Z. Y.; Li, X. D.; Xia, Y. N. *MRS Bull.* **2005**, *30*, 356–361.
(23) Liu, X.; Huang, R.; Zhu, J. *Chem. Mater.* **2008**, *20*, 192–197.
(24) Hofmeister, H.; Nepijko, S. A.; Ievlev, D. N.; Schulze, W.; Ertl, G. *J. Cryst. Growth* **2002**, *234*, 773–781.
(25) Chen, D. L.; Gao, L. *J. Cryst. Growth* **2004**, *264*, 216–222.
(26) Gao, Y.; Song, L.; Jiang, P.; Liu, L. F.; Yan, X. Q.; Zhou, Z. P.; Liu, D. F.; Wang, J. X.; Yuan, H. J.; Zhang, Z. X.; Zhao, X. W.; Dou, X. Y.; Zhou, W. Y.; Wang, G.; Xie, S. S.; Chen, H. Y.; Li, J. Q. *J. Cryst. Growth* **2005**, *276*, 606–612.
(27) Chen, H. Y.; Gao, Y.; Zhang, H. R.; Liu, L. B.; Yu, H. C.; Tian, H. F.; Xie, S. S.; Li, J. Q. *J. Phys. Chem. B* **2004**, *108*, 12038–12043.
(28) Chen, H. Y.; Gao, Y.; Yu, H. C.; Zhang, H. R.; Liu, L. B.; Shi, Y. G.; Tian, H. F.; Xie, S. S.; Li, J. Q. *Micron* **2004**, *35*, 469–474.
(29) Gao, Y.; Jiang, P.; Liu, D. F.; Yuan, H. J.; Yan, X. Q.; Zhou, Z. P.; Wang, J. X.; Song, L.; Liu, L. F.; Zhou, W. Y.; Wang, G.; Wang, C. Y.; Xie, S. S.; Zhang, J. M.; Shen, A. Y. *J. Phys. Chem. B* **2004**, *108*, 12877–12881.
(30) Sun, Y. G.; Mayers, B.; Herricks, T.; Xia, Y. N. *Nano Lett.* **2003**, *3*, 955–960.
(31) Kong, X. Y.; Ding, Y.; Yang, R.; Wang, Z. L. *Science* **2004**, *303*, 1348–1351.
(32) Frenken, J. W. M.; Stoltze, P. *Phys. Rev. Lett.* **1999**, *82*, 3500–3503.
(33) Hollingsworth, M. D. *Science* **2002**, *295*, 2410–2413.
(34) Iijima, S.; Ichihashi, T. *Phys. Rev. Lett.* **1986**, *56*, 616.
(35) Smith, D. J.; Petford-Long, A. K.; Wallenberg, L. R.; Bovin, J.-O. *Science* **1986**, *233*, 872–875.

CG701128B